

Evaluation of April Tag and WhyCode Fiducial Systems for Autonomous Precision Drone Landing with a Gimbal-Mounted Camera

Joshua Springer, Marcel Kyas
Reykjavik University

Abstract— Fiducial markers provide a computationally cheap way for drones to determine their location with respect to a landing pad and execute precision landings. However, most existing work in this field uses a fixed, downward facing camera that does not leverage the common gimbal-mounted camera setup found on many drones. Such rigid systems cannot easily track detected markers, and may lose sight of the markers in non-ideal conditions (e.g. wind gusts). This paper evaluates April Tag and WhyCode fiducial systems for drone landing with a gimbal-mounted, monocular camera, with the advantage that the drone system can track the marker over time. However, since the orientation of the camera changes, we must know the orientation of the marker, which is unreliable in monocular fiducial systems. Additionally, the system must be fast. We propose 2 methods for mitigating the orientation ambiguity of WhyCode, and 1 method for increasing the runtime detection rate of April Tag. We evaluate our 3 systems against 2 default systems in terms of marker orientation ambiguity, and detection rate. We test rates of marker detection in a ROS framework on a Raspberry Pi 4, and we rank the systems in terms of their performance. Our first WhyCode variant significantly reduces orientation ambiguity with an insignificant reduction in detection rate. Our second WhyCode variant does not show significantly different orientation ambiguity from the default WhyCode system, but does provide additional functionality in terms of multi-marker WhyCode bundle arrangements. Our April Tag variant does not show performance improvements on a Raspberry Pi 4.

I. INTRODUCTION

Precision drone landing methods employ extra sensing, e.g. terrain analysis or detection of marked landing sites, to improve on the relatively low accuracy of GPS-based landing. One prevalent type of precision landing depends on visual fiducial markers, such as those shown in Figure 1, to determine the *pose* (position + orientation) of a landing pad using a monocular camera. [1], [2], [3], [4] These methods fix the orientation of the camera to look straight down, so that the drone can approach using only the *position* of the marker, while ignoring its unreliable *orientation*. However, the fixed orientation of the camera makes it easy for the system to lose sight of the marker in adverse conditions such as wind. We work towards a method of precision landing that leverages a movable, gimbal-mounted camera to track landing pads over time, which helps a drone to maintain view of the landing pad in adverse conditions. This requires that we consider the full pose of the fiducial markers, including their orientations, since the orientation of the camera changes.

We contribute 3 custom variants of the April Tag and WhyCode fiducial systems, and an evaluation of them against the original April Tag and WhyCode variants as baselines,

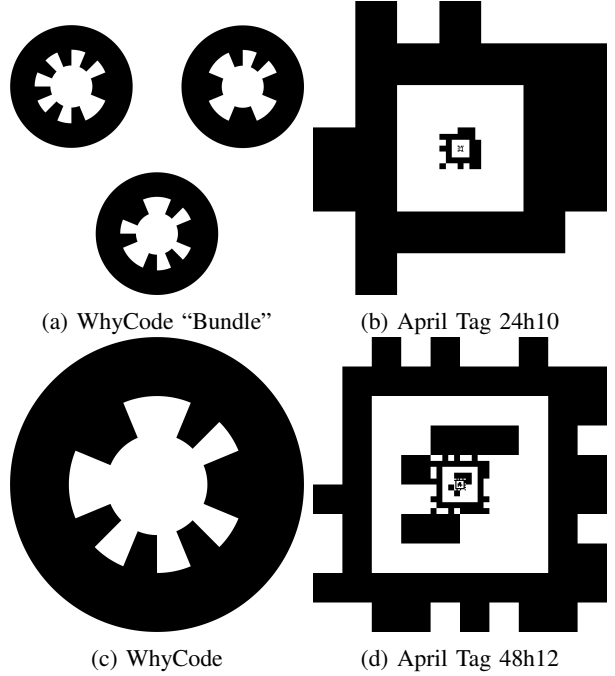


Fig. 1: The fiducial markers evaluated in this paper.

in terms of detection rate and orientation ambiguity (the tendency of the system to have sign flips and other spikes in its detected orientations). We use this information to choose a marker system for a precision landing algorithm that depends on a gimbal-mounted camera, and can thereby provide marker tracking. This algorithm assumes that the gimbal provides no data describing its own orientation, as this is the case with many common gimbals - especially those that provide stabilization, and therefore do not have a one-to-one relation between their control signal and orientation. With this assumption, the orientation of the fiducial marker must be used to estimate the position of the drone relative to the marker. We examine multiple methods for overcoming the issue of orientation ambiguity that is inherent in the monocular detection of fiducial markers.

We focus on monocular fiducial systems (instead of other viable options) because they require only a monocular camera (arguably the most common drone peripheral sensor), they are computationally cheap and can therefore execute on embedded hardware onboard a drone, they do not add behavioral constraints, unlike e.g. optical flow terrain analysis which requires motion, and they are cheap to deploy,

requiring only a printout of a particular marker. There are many possible fiducial systems [5], [6], [7], [8], [9], but we choose those that are highly configurable, open source, and whose positional accuracy has been formally evaluated. Some systems that address the issue of orientation ambiguity (such as Lentinmark [10] and the filtering method described in [11]) involve fundamental changes to existing, widely used marker systems, and they are therefore less widely used. We aim to produce simpler solutions that require minimal changes to existing marker systems in order to allow easy integration. Figures 1a-1d show the evaluated markers.

II. BACKGROUND

Fiducial markers are 2-dimensional patterns whose positions can accurately be determined in space using only images. They typically encode some information such as an ID number. Most fiducial systems do not have a notion of time, but instead analyze each video frame independently. WhyCode [7] (shown in Figure 1a and 1c) is a lightweight, circular fiducial marker system, formed by an inner white circle, outer black circle, and a Manchester encoded ID between the two circles. April Tag [9][12][13] (shown in Figures 1b and 1d) is a square marker system with a configurable layout white and black squares, each representing a data bit or a section of the black and white border.

It is difficult to determine the orientation of planar fiducial markers using single-image, monocular systems, due to the fact that a marker may have the same appearance when viewed from specific, different angles. This orientation ambiguity typically results in apparent discontinuities in a marker's orientation when it is viewed as a time series. If the full marker pose (position + orientation) is used as a control input to the drone, these discontinuities can cause potentially destructive, erratic behavior. Therefore, it is easier to achieve stable precision drone landing using a fixed, downward-facing camera, so that the control algorithm needs only to consider the position of the fiducial marker and can ignore its orientation. Conversely, a marker system that avoids these discontinuities would enable gimbal-based marker tracking and therefore more reliable precision landing.

III. RELATED WORK

Several projects have accomplished autonomous precision drone landing with fiducial markers and a *fixed* camera. Wynn [1] uses ArUco markers to land on a ship after an initial GPS-based approach, with a smaller marker nested inside a larger marker for more detection range. Borowczyk et al. [4] use a single April Tag marker, with multiple GPS receivers and data links to land a DJI Matrice on a moving ground vehicle. Falanga et al. [2] use 2 fixed cameras and a specially designed marker to land a drone on a moving platform indoors. Wubben et al. [3] use a single downward-facing camera and 2 non-nested ArUco [6] markers to identify and land on a landing pad, reporting some losses in marker detection as a result of wind pushing the drone during landing. In the above projects, the fixed camera allows the landing system to consider only the position of the

marker's pose (since the orientation of the camera is known), and not its orientation, thereby eliminating the problem of orientation ambiguity. However, the fixed camera also makes it more difficult to track the markers, since multi-rotor drones change orientation in order to vector their thrust. We evaluate the orientation ambiguity of our systems to determine if they are applicable in a gimbaled setting to allow for marker tracking, thereby increasing reliability of the landing method.

Irmisch [14] has analyzed the performance of April Tag and WhyCon markers in terms of their abilities to determine correct *position*, but not *orientation*, in real world experiments. The experiments show that both April Tag and WhyCon have relatively low position estimate errors. The issue of ambiguity in planar marker orientation is a known problem, and various methods exist which attempt to mitigate it. One example is an edition of ARTag called LentiMark [10], which uses special Moiré patterns on the outside of the tags to determine a correct orientation. Another study [11] proposes to determine the correct solution using an averaging algorithm with multiple views of the markers, instead of using only a single image. The method in [15] proposes to consider the marker as a moving object, and therefore reduces orientation ambiguity by intelligently choosing the orientation using a motion model.

IV. METHODS

A. ROS Message Attributes and Calculations

April Tag and WhyCode both have ROS (Robot Operating System) [16] modules that allow them to interact with other programs, such as flight control software. We have extended them to perform calculations and include message attributes for drone landing:

- 1) A **position target** in the drone's "east, north, up" (ENU) coordinate frame. This parameter assumes that the marker is flat on the ground, facing up.
- 2) The **normalized pixel position** $u_n, v_n \in [-1, 1]$ of the center of each marker, which serve as inputs to the systems that track the marker.
- 3) The marker's **orientation components**: yaw, pitch, and roll. Our edits exposed these to the ROS interfaces in the cases where they were not explicitly exposed. The landing system uses the yaw to align itself to the landing pad before descent.

We use the position targets and orientation components to evaluate the systems' performance in terms of orientation recognition. The normalized pixel positions and marker names will be used in future drone landings.

B. Tested Fiducial Systems

- 1) *WhyCode Orig - Tooth Arclength Sampling*: We use a version of WhyCode created by Ulrich [17] as a baseline for testing. The method samples the ellipse that goes through the centers of the "teeth" forming the marker's ID (i.e. the yellow and green ellipses in Figure 2), to determine the marker's orientation. Of the 2 possible candidate solutions that are implied by the detected semi-axes of the outer black ellipse, the detector chooses the one that has lower variance on

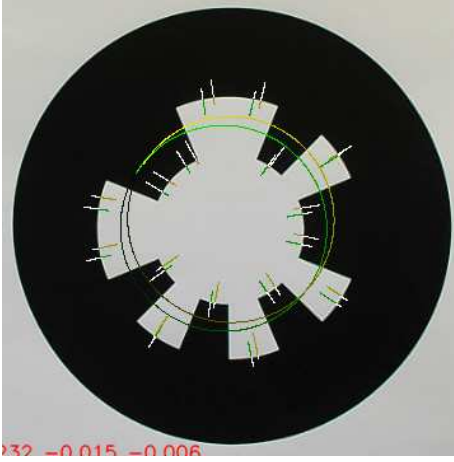


Fig. 2: An illustration of WhyCode detection. Each ellipse and corresponding radial lines represent the sampling locations, marked in yellow and green to distinguish the two candidate solutions. The WhyCode Orig method uses only the ellipses to choose a solution, while our WhyCode Ellipse method uses both the ellipse and the radial lines. In this case, the green solution is correct and is visually better centered on the marker.

the number of sample points per tooth. This works because the candidate solutions predict this ellipse to be in slightly different places, and the correct solution should predict the ellipse to be in its correct place, minimizing the variance in the number of sample points that coincide with each tooth. Conversely, the incorrect solution should predict the ellipse to be in the incorrect place, such that the sampling ellipse does not line up well with the marker, and the variance is higher. We use WhyCode markers with 8-bit IDs, so that there are several sample points and a meaningful variance.

2) *WhyCode Ellipse - Radial Tooth Sampling*: The first method that we have created for reducing orientation ambiguity is the `ellipse_sampling` branch of [18]. The method determines the marker ID and the two candidate solutions for the orientation as in WhyCode Orig, after which it identifies the lines that go from the center of the white region through the center of each tooth. It then samples the input image on these lines, as illustrated by the radial sample lines in Figure 2. It expects a white-to-black transition at the predicted edge of each tooth, and the sampling line is centered on this edge. The true edge is determined during sampling, and its value is recorded as a percentage of the length of the line segment, oriented such that 0 corresponds to the centermost end of the line segment, and 1 corresponds to its outermost end. The detector chooses the solution that minimizes the variance of the location of the true edge over the sample lines.

3) *WhyCode Multi - Planar Regression from Multiple Markers*: The second method that we have created for reducing orientation ambiguity (the `multi` branch of [18]) works under the assumption that all markers are co-planar. For each input image, the WhyCode algorithm identifies all

markers and then finds the normal vector to the plane implied by the markers' positions, after which it can calculate the pitch and roll components of the bundle's orientation. The position of the bundle is defined to be the mean of the positions of its constituent markers, and its yaw is that of any constituent markers, with the assumption they are all the same. The detector then calculates all additional attributes for the bundle as if it were a marker. This system uses an arrangement of WhyCode markers such as in Figure 1a.

4) *April Tag 48h12 - Large, Embeddable April Tag Family*: April Tag provides a default family 48h12, shown in Figure 1d, for which the 4 center squares are undefined, 20 squares provide a white border, 28 squares provide a black border, and 48 squares provide data bits, giving a total of 96 defined squares. The undefined center provides a space to embed a smaller marker, which is useful in the last stages of a drone landing scenario, where the camera is too close to the landing pad to see the larger markers. We test this family as a baseline for the performance of April Tag.

5) *April Tag 24h10 - Small, Embeddable April Tag Family*: We have created an April Tag 24h10 family (shown in Figure 1b) in response to our initial experiments, which showed that April Tag 48h12 has a slower detection rate than WhyCode on embedded hardware. We maintain marker embeddability while decreasing the size of the marker definition, by reducing the size of the undefined center to region to 1 square, and adjusting the surrounding regions accordingly: 8 squares for a white border, 16 squares for a black border, and 24 outer data squares. This gives a total of 48 defined squares (compared to the 96 squares of April Tag 48h12). We test April Tag 24h10 to see if it can offer an increase in detection rate with respect to April Tag 48h12.

C. Bases of Comparison

1) *Discontinuities*: Orientation ambiguity manifests as discontinuities (e.g. sign flips and other spikes) in the pitch and roll components of a marker's orientation. These discontinuities are also propagated to subsequent calculations that depend on the orientation - *the position targets*. The fiducial systems are compared on the basis of the number of discontinuities in the position targets they generate. A "good" system minimizes this number.

We capture 33 videos of the marker arrangement in Figure 1, printed so each marker has a side length of 30 cm, and mounted to a planar surface with clear lighting. We move the camera in each of videos (e.g. panning, tilting, moving in and out, etc.) while keeping all markers completely in frame at all times. The videos are saved as a series of pairs of image and camera info messages in the standard ROS way, using `rosbag`. Each fiducial system in Section IV-B processes the same set of videos. Since the experiments are conducted slowly in a controlled environment, angular and linear speeds above experimentally-determined thresholds can be classified as discontinuities. Linear discontinuities occur when the quotient of any position target $\vec{P} = \langle p_e, p_n, p_u \rangle$ (east, north,

or up) and its predecessor is sufficiently negative:

$$\frac{p_{x,i+1}}{p_{x,i}} < \theta_l < 0 \quad (1)$$

where $p_{x,i}$ and $p_{x,i+1}$ are position targets in a single dimension $x \in \{e, n, u\}$ dimension at frames i and $i + 1$ respectively, and $\theta_l < 0$ is an experimentally determined threshold (see Table I). If the inequality in Equation 1 is true, this implies that the marker appears to change locations faster than allowed during testing. Similarly, a discontinuity determined from angular speed s_a occurs when

$$s_a = \frac{\text{dist}(q_i, q_{i+1})}{\Delta t} > \theta_a > 0 \quad (2)$$

where q_i and q_{i+1} are the quaternions representing the orientation of a marker at frames i and $i + 1$ respectively, $\text{dist} \geq 0$ is the intrinsic geodesic distance between the angles represented by the quaternions, Δt is the change in time between frames i and $i + 1$, and θ_a is an experimentally determined threshold (see Table I). If the inequality in Equation 2 is true, this implies that the marker appears to rotate faster than allowed during testing.

We consider cases where Equations 2 and 1 are true simultaneously, to reduce false identification of discontinuities. For example, a linear discontinuity can appear erroneously via noise when some component of a marker's position target is close to 0, and a discontinuity in angular speed can be caused by quirks in the notation of the orientation of a marker, when no linear discontinuity occurs (e.g. jumping from 2π to 0 as a result of normalization). If both discontinuities occur at the same time, this means that the marker truly appears to drastically change positions in space in a small amount of time, which does not happen in our test cases. Finally, since the test cases vary in length, we can define a “discontinuity rate” $r_d = \frac{d}{n}$ which describes the number of discontinuities d as a portion of the total number of detections n , and which serves as a basis for comparing the performance of each system in each test case.

2) Detection Rate: We capture 14 videos of each marker in Figure 1 separately with both the camera and marker remaining still, at several distances and deflections from one another. We record videos of each marker in isolation, to avoid any potential interference, since the marker detectors all analyze black and white regions. Both the camera and marker remain still during each test case, and each test case lasts 60 s. The systems are compared on the basis of their detection rate (Hz) when executing on a Raspberry Pi 4, with the following ROS pipeline: replaying a test case video, image rectification using `image_proc` (April Tag systems only, required by April Tag ROS module), marker detection each of the fiducial systems in Section IV-B, and data collection for later analysis. This avoids capturing the image during testing, but maintains fairness of comparison among the systems, since all systems are put into the same computational environment one at a time, and all process similar test cases. We then determine a detection rate $F = \frac{n}{t}$, where n is the number of detections, and t is the length in seconds of the test case.

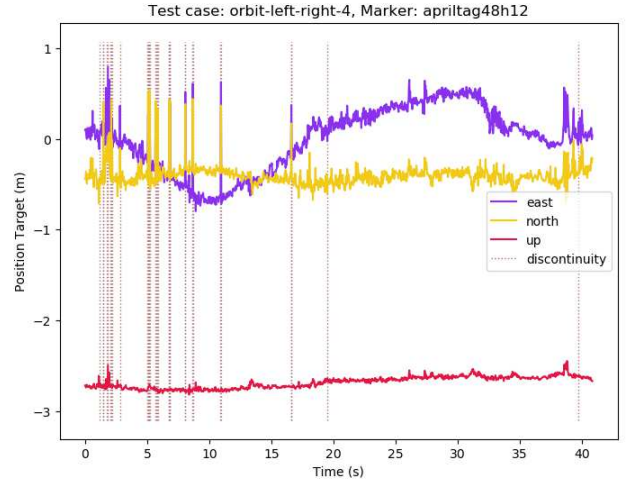


Fig. 3: Example of discontinuities in position targets (marked by the vertical lines), which are spikes in the east and north position targets that roughly correspond to sign flips.

3) Statistical Tests: We rank each system according to its discontinuity rate (lower being better), and detection rate (higher being better). First, we compare the systems as a single group using a Kruskal-Wallis H test, to test for statistical differences among all groups:

if $p_{\forall} < 0.05$, at least one system stochastically dominates at least one other system in (H1) terms of discontinuity rate.

If (H1) is true, we conduct pairwise Wilcoxon tests to determine the ranking of the system with regard to each metric. For each pair, we test whether each pair is significantly different (two-tailed):

if $p_{=} < 0.05$, one of the two systems stochastically dominates the other, (H2)

and whether the first system of the pair has a lesser discontinuity rate than the second system (one-tailed):

if $p_{\geq} < 0.05$, the first system has a lower discontinuity rate than the second system. (H3)

We conduct second set of tests with similar hypotheses to rank the systems by their detection rate, with hypotheses oriented toward a higher metric, rather than a lower one, e.g. (H3) tests whether the first system has a *higher* detection rate than the second system.

V. RESULTS

A. Discontinuities:

Figure 3 gives an intuition for the nature of the discontinuities studied in this paper. It shows the east, north, and up position targets, labeled with vertical lines when a discontinuity occurs. In the case of drone flight, the east, north, and up position targets command the drone to go right, forward, and up respectively. These discontinuities are destructive to a landing process.

Discontinuity Type	Symbol	Value
rotational	θ_a	1.0 rad/s
linear	θ_l	-0.8 (unitless)

TABLE I: Thresholds for targeting pose discontinuities in all systems. We say that a discontinuity occurs when the inequalities in Equations 1 and 2 are simultaneously true using the values in this table. These are chosen to be well above the maximum allowed values in testing, so that they are not sensitive to noise.

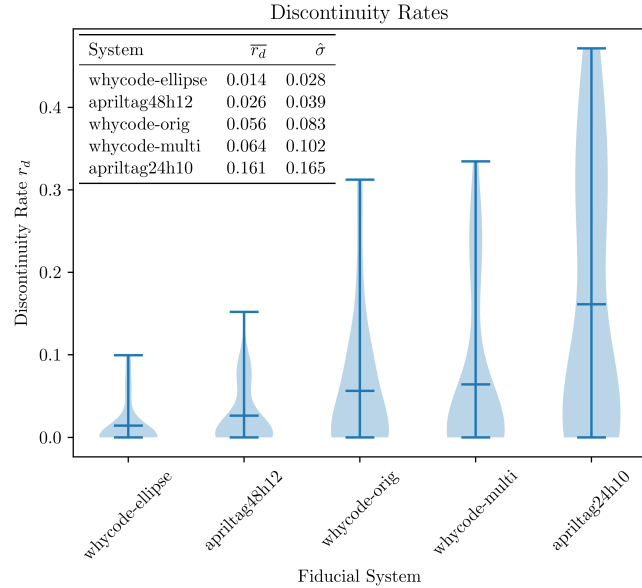


Fig. 4: A visualization of the discontinuity rates r_d , which represent the proportion of discontinuous position target readings relative to the total number of readings. \bar{r}_d is the sample mean of the discontinuity rate, and $\hat{\sigma}$ is the sample standard deviation, and $n = 33$ per group.

Table I shows the speed thresholds for Equations 1 and 2. Table II presents the results of a Kruskal-Wallis test on the discontinuity rates, concluding that the systems are *not* all equal. Table III presents the results of pairwise Wilcoxon tests to rank the systems against one another. It concludes that WhyCode Ellipse has a lower discontinuity rate than all other systems except April Tag 48h12, and that all systems have a lower discontinuity rate than April Tag 24h10. The other pairwise comparisons are inconclusive, meaning that they detect no significant statistical difference. Figure 4 visualizes the discontinuity rates for each system.

B. Detection Rates

Table IV presents the results of a Kruskal Wallis test on the detection rates, concluding that the systems are *not* all equal.

$p_{\forall=}$	H
0.000033	25.935888

TABLE II: Kruskal-Wallis test on the discontinuity rates.

System 1	System 2	$p_{\forall=}$	$U_{\forall=}$	p_{\geq}	U_{\geq}
whycode-ellipse	apriltag48h12	0.178	167		
whycode-ellipse	whycode-orig	0.003	34	0.001	34
whycode-ellipse	whycode-multi	0.027	106	0.014	106
whycode-ellipse	apriltag24h10	0.000	49	0.000	49
apriltag48h12	whycode-ellipse	0.178	167		
apriltag48h12	whycode-orig	0.139	149		
apriltag48h12	whycode-multi	0.245	176		
apriltag48h12	apriltag24h10	0.001	89	0.001	89
whycode-orig	whycode-ellipse	0.003	34	0.999	219
whycode-orig	apriltag48h12	0.139	149		
whycode-orig	whycode-multi	0.861	224		
whycode-orig	apriltag24h10	0.008	123	0.004	123
whycode-multi	whycode-ellipse	0.027	106	0.986	300
whycode-multi	apriltag48h12	0.245	176		
whycode-multi	whycode-orig	0.861	224		
whycode-multi	apriltag24h10	0.004	100	0.002	100
apriltag24h10	whycode-ellipse	0.000	49	1.000	447
apriltag24h10	apriltag48h12	0.001	89	0.999	439
apriltag24h10	whycode-orig	0.008	123	0.996	405
apriltag24h10	whycode-multi	0.004	100	0.998	396

TABLE III: Wilcoxon tests on the discontinuity rates.

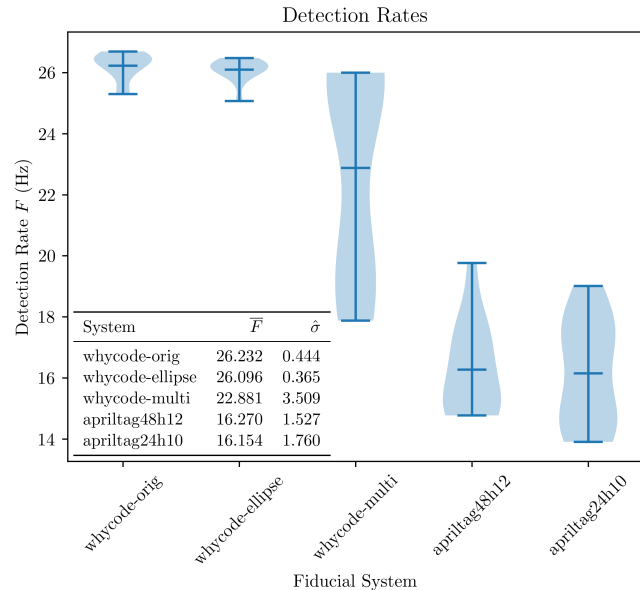


Fig. 5: A visualization of the detection rates F (Hz). \bar{F} is the sample mean of the detection rate, and $\hat{\sigma}$ is the sample standard deviation, and $n = 14$ per group.

Table V presents the results of pairwise Wilcoxon tests on the detection rates to rank the systems against one another, concluding that the detection rates of WhyCode Orig and WhyCode ellipse are not significantly different from each other, but are higher than all other systems, that WhyCode Multi has a higher detection rate than the April Tag systems, and that April Tag 48h12 and April Tag 24h10 have the lowest detection rates and are not significantly different.

VI. DISCUSSION

WhyCode Ellipse offers a significant decrease in discontinuity rate compared to WhyCode Orig, with a non-significant decrease in detection rate. WhyCode Multi does not offer a

$p_{\forall}=$	H
2.275795e-11	55.737741

TABLE IV: Kruskal-Wallis H Test on the detection rates.

System 1	System 2	$p_{\forall}=$	$U_{\forall}=$	p_{\leq}	U_{\leq}
whycode-orig	whycode-ellipse	0.158	30		
whycode-orig	whycode-multi	0.001	0	1.000	105
whycode-orig	apriltag48h12	0.001	0	1.000	105
whycode-orig	apriltag24h10	0.001	0	1.000	105
whycode-ellipse	whycode-orig	0.158	30		
whycode-ellipse	whycode-multi	0.004	7	0.998	98
whycode-ellipse	apriltag48h12	0.001	0	1.000	105
whycode-ellipse	apriltag24h10	0.001	0	1.000	105
whycode-multi	whycode-orig	0.001	0	0.000	0
whycode-multi	whycode-ellipse	0.004	7	0.002	7
whycode-multi	apriltag48h12	0.001	0	1.000	105
whycode-multi	apriltag24h10	0.001	0	1.000	105
apriltag48h12	whycode-orig	0.001	0	0.000	0
apriltag48h12	whycode-ellipse	0.001	0	0.000	0
apriltag48h12	whycode-multi	0.001	0	0.000	0
apriltag48h12	apriltag24h10	0.975	52		
apriltag24h10	whycode-orig	0.001	0	0.000	0
apriltag24h10	whycode-ellipse	0.001	0	0.000	0
apriltag24h10	whycode-multi	0.001	0	0.000	0
apriltag24h10	apriltag48h12	0.975	52		

TABLE V: Pairwise Wilcoxon tests on the detection rates.

decrease in discontinuity rate compared to WhyCode Orig, but does have a lower detection rate. Therefore, according to the metrics we consider, it is not an improvement. However, it shows that the notion of a marker “bundle” can be extended to WhyCode, and this opens up possibilities for pseudo-embedded marker arrangements in the future. April Tag 24h10 offers a significant increase in discontinuity rate compared to April Tag 48h12, with no increase in detection rate. The lower detection rates of the April Tag systems are likely a result of their longer ROS pipeline, which depends on transmitting each input image to an intermediate `image_proc` node and back for rectification. WhyCode builds this into its algorithm, thereby avoiding latency and performing faster than April Tag even when detecting several markers at a time. However, WhyCode systems cannot handle marker embedding as April Tag systems can.

A threat to validity for this study is that we have tested the systems with default runtime parameters and a single hardware setup, while there is a practically infinite space of parameters and hardware setups that can influence the performance of the systems. Still, this study provides a baseline for future analysis.

VII. CONCLUSION

We have evaluated 5 fiducial systems - 2 existing variants: April Tag 48h12 and WhyCode Orig, and 3 custom variants which we have created - in terms of their rates of discontinuity in position target generation and detection rate. We have determined that WhyCode Ellipse, WhyCode Multi, April Tag 48h12, and WhyCode Orig provide a good starting point for testing gimbal-based fiducial landing with a drone, while April Tag 24h10 is likely to exhibit problematic behavior.

VIII. FUTURE WORK

The marker systems in this paper will be further tested for autonomous precision landing on a real drone, where the orientation ambiguity can be destructive and a high framerate is key. Future tests of the WhyCode Multi system could include multi-size, multi-marker arrangements to mimic marker embedding. Future tests of all systems could include different runtime parameters, hardware setups, lighting conditions, etc.

REFERENCES

- [1] J. S. Wynn, “Visual Servoing for Precision Shipboard Landing of an Autonomous Multirotor Aircraft System,” Master’s thesis, Brigham Young University, 9 2018. [Online]. Available: <http://hdl.lib.byu.edu/1877/etd10385>
- [2] D. Falanga, A. Zanchettin, A. Simovic, J. Delmerico, and D. Scaramuzza, “Vision-based autonomous quadrotor landing on a moving platform,” 10 2017.
- [3] J. Wubben, F. Fabra, C. Calafate, T. Krzeszowski, J. Marquez-Barja, J.-C. Cano, and P. Manzoni, “Accurate Landing of Unmanned Aerial Vehicles Using Ground Pattern Recognition,” *Electronics*, vol. 8, p. 1532, 12 2019.
- [4] A. Borowczyk, D.-T. Nguyen, A. Phu-Van Nguyen, D. Q. Nguyen, D. Saussié, and J. L. Ny, “Autonomous Landing of a Multirotor Micro Air Vehicle on a High Velocity Ground Vehicle,” *IFAC-PapersOnLine*, vol. 50, no. 1, pp. 10 488–10 494, 2017, 20th IFAC World Congress.
- [5] M. Fiala and M. Fiala, “ARTag, a fiducial marker system using digital techniques,” in *Proceedings of the 2005 IEEE Computer Society Conference on Computer Vision and Pattern Recognition (CVPR’05) - Volume 2 - Volume 02*, ser. CVPR ’05. Washington, DC, USA: IEEE Computer Society, 2005, pp. 590–596.
- [6] S. Garrido-Jurado, R. Muñoz-Salinas, F. Madrid-Cuevas, and M. Marín-Jiménez, “Automatic generation and detection of highly reliable fiducial markers under occlusion,” *Pattern Recognition*, vol. 47, p. 2280–2292, 06 2014.
- [7] P. Lightbody, T. Krajník, and M. Hanheide, “A Versatile High-performance Visual Fiducial Marker Detection System with Scalable Identity Encoding,” in *Proceedings of the Symposium on Applied Computing*, ser. SAC ’17. New York, NY, USA: ACM, 2017, pp. 276–282.
- [8] M. Nitsche, T. Krajník, P. Čížek, M. Mejail, and T. Duckett, “Whycon: An efficient, marker-based localization system,” in *IROS Workshop on Open Source Aerial Robotics*, 2015. [Online]. Available: <https://core.ac.uk/download/pdf/42583963.pdf>
- [9] E. Olson, “AprilTag: A Robust and Flexible Visual Fiducial System,” in *2011 IEEE International Conference on Robotics and Automation*, 2011, pp. 3400–3407.
- [10] H. Tanaka, Y. Sumi, and Y. Matsumoto, “A solution to pose ambiguity of visual markers using Moiré patterns,” in *2014 IEEE/RSJ International Conference on Intelligent Robots and Systems*, 2014, pp. 3129–3134.
- [11] S.-F. Ch’ng, N. Sogi, P. Purkait, T.-J. Chin, and K. Fukui, “Resolving Marker Pose Ambiguity by Robust Rotation Averaging with Clique Constraints,” 2019.
- [12] J. Wang and E. Olson, “Apriltag 2: Efficient and robust fiducial detection,” 10 2016, pp. 4193–4198.
- [13] M. Kröglis, A. Haggemiller, and E. Olson, “Flexible layouts for fiducial tags,” in *2019 IEEE/RSJ International Conference on Intelligent Robots and Systems (IROS)*, 2019, pp. 1898–1903.
- [14] P. Irmisch, “Camera-based Distance Estimation for Autonomous Vehicles,” 12 2017.
- [15] P.-C. Wu, Y.-H. Tsai, and S.-Y. Chien, “Stable pose tracking from a planar target with an analytical motion model in real-time applications,” 11 2014.
- [16] M. Quigley, K. Conley, B. Gerkey, J. Faust, T. Foote, J. Leibs, R. Wheeler, and A. Ng, “ROS: an open-source Robot Operating System,” vol. 3, 01 2009.
- [17] J. Ulrich, “Fiducial Marker Detection for Vision-based Mobile Robot Localisation,” pp. 18–21, 2020, bachelor Thesis.
- [18] Joshua Springer. (2020) Edited WhyCon/WhyCode Repository. “<https://github.com/uzgit/whycon-ros>”. (accessed: 2022.2.2). [Online]. Available: <https://github.com/uzgit/whycon-ros>